Journal of Catalysis **206,** 143–154 (2002)
doi:10.1006/jcat.2001.3475, available online at http://www.idealibrary.com on IDEAL®

Environmental Catalysis on Iron Oxide–Silica Aerogels: Selective Oxidation of NH_3 and Reduction of NO by NH_3

P. Fabrizioli, T. Bürgi, and A. Baiker[1]

Laboratory of Technical Chemistry, Swiss Federal Institute of Technology, ETH Hönggerberg-HCI, CH-8093 Zürich, Switzerland

Received September 13, 2001; revised November 15, 2001; accepted November 19, 2001

The catalytic properties of mesoporous iron oxide–silica aerogels prepared by a sol–gel process combined with ensuing supercritical extraction with CO_2 was investigated in the selective oxidation (SCO) of ammonia and the selective reduction (SCR) of NO by ammonia. The main parameters changed in the aerogel preparation were the type of base used as gelation agent, the iron content, and the calcination temperature. The aerogels differed significantly in acidity and iron dispersion. Diffuse reflectance infrared Fourier transform spectroscopy studies of ammonia adsorption at different temperatures revealed that ammonia was bound to Brønsted- and Lewis-type sites, the latter being dominant at 300°C. A fraction of low coordinated Fe^{2+} sites were probed by NO adsorption measurements. Lewis-type sites were found to be associated with low-coordinated iron sites. Catalytic tests were performed in a continuous fixed-bed reactor in the temperature 210–550°C range and at ambient pressure. The catalytic activity of the aerogels in SCO correlated with the abundance of more strongly bound ammonia adsorbed on Lewis sites (low coordinated iron). High selectivity to nitrogen (97%) could be reached up to 500°C, whereas at higher temperature the formation of N_2O and NO became significant. The apparent activation energy of N_2 formation ranged from 69 to 94 kJ/mol, whereby catalysts with higher selectivity and activity showed lower activation energy. In SCR, selectivity to nitrogen was for all aerogels >98% at T < 460°C, and activation energies varied from 38 to 53 kJ/mol. The catalytic activity for SCR did not correlate with the population density of Lewis sites. We propose that SCO predominantly occurs on Lewis sites consisting of highly dispersed iron atoms of low coordination, whereas in SCR these sites do not play an important role.

Key Words: **iron oxide–silica aerogels; selective oxidation of ammonia; selective reduction of NO; supercritical drying; Brønsted and Lewis acidity.**

1. INTRODUCTION

Iron–silicon oxide-based materials have received considerable attention as potential catalysts for reactions relevant to environmental and petrochemical catalysis. This is most prominently demonstrated by the family of crystalline iron silicalites (1), which have been reported to possess interesting catalytic potential in a variety of reactions. Indeed, the acid properties of the incorporated Fe^{3+} and the redox properties of finely dispersed iron oxide particles, together with shape selectivity of the zeolite, are attractive properties for catalytic application (1). Comparatively little attention has been given to supported iron oxide (2–5) and to iron–silicon oxide aerogels: Wang and Willey (6) synthesized high-temperature Fe_2O_3–SiO_2 aerogels for the oxidation of methanol. Willey *et al.* prepared iron oxide–chromia–alumina high-temperature aerogels (7), and magnesium oxide–iron oxide spinel aerogels (8) for the selective catalytic reduction of NO by ammonia. No report deals with iron oxide–silica aerogels, prepared by low-temperature extraction with supercritical CO_2.

Aerogels can offer high flexibility in the tuning of the textural properties and chemical composition, as has been exemplified for the titania–silica-mixed oxides used for the epoxidation of olefins (9). A problem inherent to the sol–gel-derived materials is, however, that mixing of the constituents on the molecular scale is often not perfect, and real "single-site" catalysts are difficult to achieve. Nevertheless comparative studies of titania silicalites and titania–silica aerogels proved that the catalytic properties of the amorphous aerogels are in some cases outperforming those of the crystalline materials (10). This prompted us to explore the potential of iron oxide–silica aerogels in catalysis.

In a preceding study (11) we reported on the synthesis and chemical and structural properties of iron oxide–silica aerogels. Here we address the catalytic properties of these materials. Two environmentally relevant reactions are the focus of our study: the selective catalytic oxidation (SCO) of ammonia and the selective catalytic reduction (SCR) of NO_x by ammonia. The latter is the most frequently used technique to eliminate NO_x from oxygen-containing waste gases of stationary combustion sources. Although various catalysts were applied for this reaction (12), most attention has been given to vanadia- on titania-based catalysts. Comparatively little is known about the catalytic performance of iron-containing catalysts, such as iron-exchanged zeolites

[1] To whom correspondence should be addressed. Fax: 41 1 632 11 63. E-mail: baiker@tech.chem.ethz.ch.

0021-9517/02 $35.00

(13–17), pillared clays (18–20), mixed oxides (8, 21), and supported iron oxides (4, 5, 22, 23).

In practice, the SCO to nitrogen succeeds the SCR unit, where the gas exits with a temperature of 280–480°C. SCO of ammonia to nitrogen also finds application in the treatment of reformates for fuel-cell systems and in the deodorization of ammonia-containing gas (24, 25). Iron-containing catalysts applied in SCO include ferrisilicate and Fe-exchanged zeolites (16, 26, 27), supported iron oxide catalysts (3, 28–30), and pure iron oxides (31–33). As for SCR, iron oxide–silica aerogels are novel catalyst materials for this reaction.

2. EXPERIMENTAL

2.1. Preparation and Characterization of Aerogels

The preparation and structural and chemical properties of iron oxide–silica aerogels used in this work were described in detail elsewhere (11). In brief, aerogels were prepared from tetramethoxysilicon(IV) or tetraethoxysilicon(IV) and $Fe(NO_3)_3 \cdot 9\,H_2O$ using a sol–gel process with different nitrogen-containing bases (*N*,*N*-diethylaniline, trihexylamine, ammonium hydroxide, ammonium carbonate) as gelation agents. The gels were dried by extraction of the solvent with supercritical CO_2 at 40°C and 22 MPa and calcined in air at 600 and 900°C, respectively, before catalytic tests. The acronyms used for the gels in this work are the same as those used in a previous study (11). The first numeral refers to the nominal Fe_2O_3 content in weight percent, based on the theoretical system Fe_2O_3–SiO_2. The subsequent capital letters describe the sol–gel route applied: first the silicon precursor is given, M indicates that tetramethoxysilicon was used, and E stands for the tetraethoxysilicon precursor. The "Md" aerogels were prepared by using a higher amount of alcohol in the hydrolysis as compared to the other aerogels. Then the gelation agent is represented by two to four letters, "NN" standing for *N*,*N*-diethylaniline; "Tri," for trihexylamine, "NC," for ammonium carbonate, "NH_3," for ammonium hydroxide; "NH_3d," indicating a more diluted ammonia solution. Note that the iron content is omitted in the acronym for the gels with a nominal composition of 10 wt% Fe_2O_3/90 wt% SiO_2. Aerogels with iron content from 0 to 20 wt% Fe_2O_3 were prepared following the synthesis route of Md/NN. Calcination of the aerogel Md/NN in air at 900°C leads to sample Md/NN900.

2.2. Characterization

In addition to the previously used characterization methods (11), which included nitrogen adsorption, X-ray diffraction (XRD), transmission electron microscopy (TEM), temperature programmed reduction (TPR), X-ray photoelectron spectroscopy (XPS), UV–vis, diffuse reflectance infrared Fourier transform spectroscopy (DRIFTS), and electron paramagnetic resonance(EPR) spectroscopy, we applied temperature-programmed desorption (TPD) combined with DRIFTS for the study of ammonia and nitric oxide adsorption.

DRIFT spectra were recorded on a Perkin–Elmer 2000 FTIR instrument with a diffuse reflectance cell and a controlled environmental chamber (both Spectra-Tech) equipped with CaF_2 windows. The sample was mounted on a ceramic frit (Al_2O_3), which could be heated to elevated temperature via a PID controller (Tecon 501). Argon (Pangas, 99.999%) and synthetic air (Pangas, 20% O_2 purity 99.5%, 80% N_2 purity 99.995%) was passed through a cooling trap with an isopropanol–dry ice mixture. The DRIFT spectra in the reflection mode were transformed to the Kubelka–Munk function. Then they were normalized to the silica overtone vibration at 1848 cm^{-1}(combination mode of Si–O vibrations), as proposed by Vansant *et al.* (34). To visualize the species resulting from NH_3 or NO adsorption, the spectrum of the unloaded catalyst was substracted.

During TPD of the species adsorbed after reaction and during temperature-programmed reduction by ammonia, gas flow composition was analyzed online using a Balzers quadrupole mass spectrometer QMA 112A.

Four types of measurements were carried out.

1. NH_3 adsorption and TPD on the calcined catalysts. Prior to ammonia adsorption the catalyst was heated in a synthetic air stream (50 ml min^{-1}) to 300°C for 1 h. The air stream was dried in the cooling trap. Ammonia (Pangas, 3600 ppm in argon, dried over a KOH-containing cartridge) was adsorbed at 50°C. Thereafter the cell was flushed with argon for 2.5 h. Temperature-programmed desorption of ammonia (NH_3-TPD) was performed at a rate of 5°C min^{-1}; spectra were taken by accumulating 50 scans at a resolution of 4 cm^{-1} every 50°C.

2. NO adsorption and NO-TPD on the reduced catalysts. The aerogels M/NN, M/Tri, M/NC, M/NH_3, and E/NH_3 were used for NO adsorption studies. The catalysts were pretreated at 425°C in pure hydrogen for 20 min in the *in situ* DRIFTS cell. Then cooled down to 50°C, flushed with argon, and 2000 ppm NO/ Ar was admitted to the cell with a continuous flow of 50 ml/min. All gases were dried by means of a cooling trap (CO_2–isopropanol). The pressure in the cell was set to 2 bar by using an adjustable relief valve at the outlet of the cell. After 2 h the gas flow was changed back to argon. The cell was then flushed for 4–5 h before the steady-state spectra under Ar were recorded.

3. TPD and TPR by ammonia. TPD of the adsorbed species after SCO was performed by flushing the reactor with 50 ml/min argon at 50°C for 3 h. Thereafter the catalyst was heated at 10°C/min, and desorbing species were monitored by mass spectrometry. For comparison, TPD of ammonia from the calcined and reduced M/NN were

also measured. The aerogel was pretreated at 550°C in synthetic air and in 10% H_2/Ar (Pangas), respectively. TPR of the catalysts M/NH_3, E/NH_3, and Md/NN after use in SCO and after pretreatment in air at 550°C was investigated in 50 ml/min of 2000 ppm NH_3 in a helium (99.999%) balance (3600 ppm NH_3/He, certified ±2%, Carbagas) at a heating rate of 10°C/min in the temperature 50–550°C range.

4. DRIFTS *in situ* catalytic studies. To investigate the role of the acid sites in the SCO of ammonia, *in situ* DRIFTS studies with catalysts M/NN and E/NH_3 were performed. The catalysts were pretreated in air at 400°C, cooled to 250°C, and a background spectrum was taken. After adsorption of ammonia (3600 ppm/Ar, 50 ml/min) for 30 min, the gas flow was changed to argon, and the catalysts were flushed for 3 h. The oxidation of the adsorbed ammonia was then started by introducing 50 ml/min 1.8% O_2/Ar into the cell. Spectra were taken in 2-min intervals during the first 10 min. Then every 10 min a spectrum was taken by accumulating 100 scans at a resolution of 4 cm^{-1}.

2.3. Catalytic Tests

Catalytic tests for the SCO of NH_3 and the SCR of NO by NH_3 were carried out in a continuous-flow fixed-bed microreactor made of a 4-mm-i.d. quartz glass tube. Volumes of 0.126 cm^3 corresponding to 56–90 mg of catalyst (particle size, 65–120 μm; except for M/NH_3, E/NH_3, E/NH_3d, 120–300 μm) were used for the measurements. The reaction gas mixture for SCO consisted of 2000 ppm NH_3 and 2.0% O_2 in a helium balance, whereas for SCR of NO, 900 ppm NO, 900 ppm NH_3, and 1.8% O_2 were mixed. The gas mixture was made from single-component gases in a helium (99.999%) balance (3600 ppm NH_3/He, 2000 ppm NO/He, 7% O_2/He certified ±2%, Carbagas). Feed and product concentrations of NH_3, N_2, NO, N_2O, and O_2 were quantitatively analyzed online using a Balzers quadrupole mass spectrometer QMA 112A.

Conversion measurements as a function of temperature were carried out at a gas-hourly space velocity, GHSV, of 24,000 h^{-1} (0°C, 1 atm; standard temperature and pressure (STP)) after pretreatment of the catalysts in synthetic air (Pangas, 20% O_2 purity 99.5%, 80% N_2 purity 99.995%; 50 ml min^{-1}) at 550°C for 30 min. The pressure drop over the catalyst bed was below 0.13 bar at room temperature. For differential activity measurements the space velocity was gradually raised from 17,000 to 50,000 h^{-1} (STP), and the temperature was adjusted to keep the ammonia conversion below 20% to approximate differential reactor conditions. Turnover frequency (TOF) calculations were referred to the bulk iron content. For every measurement a balance over all nitrogen-containing compounds was calculated. Even for high conversions of ammonia, the deviation in the balance did not exceed ±3%, indicating that all species, consumed or formed, were accounted for.

3. RESULTS

3.1. Structural and Chemical Properties

The structural and chemical properties of the FeO_x/SiO_2 aerogels have been reported in detail in Ref. (11). Table 1 summarizes the main textural and chemical properties of the aerogels. Briefly, different aerogels were synthesized by varying the nitrogen-containing base, the silicon precursor, and the iron content in a sol–gel process. After calcination in air at 600°C all aerogels with 10 wt% nominal Fe_2O_3 were amorphous with pore volumes ranging from 0.7 to 2.0 cm^3 g^{-1} and surface areas between 300 and 636 m^2 g^{-1}. The pore size ranged from micro- to mesopores, and the maximum of the pore size distribution was between 20 and 50 nm. The iron ions had a mean oxidation state of about 3+. Reduction to metallic iron by hydrogen occurred only at 700–1100°C, due to strong interaction with the silica matrix. Electron spin resonance (ESR) and UV–vis spectroscopy revealed that different iron sites exist in the aerogels, ranging from isolated tetrahedrally coordinated iron ions to iron oxide clusters, depending on the sol–gel process conditions, the iron content, and the thermal treatment. Tetrahedral coordinated iron was detected in all aerogels, except those calcined at high temperature (900°C) and with high iron content (17 wt%, sample 20/Md/NN). For these samples the presence of some crystalline γ-Fe_2O_3 or $Fe_3O_4$was indicated by XRD.

TABLE 1

Structural Properties of Iron Oxide–Silica Mixed Oxide Aerogels [a]

Aerogel	S_{BET} (m^2 g^{-1})	V_P [b] (cm^3 g^{-1})	d_{max} [c] (nm)	XRD [d]
M/NN	310	1.10	40	a
Md/NN	300	0.72	23	a
Md/NN900	150	0.68	30	γ-Fe_2O_3 or Fe_3O_4
5/Md/NN	610	1.80	45	a
20/Md/NN	342	0.12	<2	γ-Fe_2O_3 or Fe_3O_4
0/Md/NN	739	2.60	40	—
M/Tri	335	0.72	20	a
M/NC	360	0.97	45	a
M/NH_3	480	1.56	43	a
E/NH_3	636	1.73	38	a
E/NH_3d	625	2.05	50	a

[a] Ref. (11). Note that samples with no numerals in acronyms contained 10 wt% nominal Fe_2O_3.

[b] V_P designates the BJH cumulative desorption pore volume of pores in the maximum diameter range 1.7–300 nm.

[c] d_{max} is the graphically assessed pore size maximum of the pore size distribution derived from the adsorption branch.

[d] XRD patterns observed. "a" stands for amorphous samples; aerogels Md/NN900 and 20/Md/NN were also predominantly amorphous but contained crystalline domains of γ-Fe_2O_3 or Fe_3O_4 not distinguishable by XRD.

3.2. DRIFTS Studies

Ammonia adsorption. Ammonia adsorption was studied to gain information about the surface acidity of the iron oxide–silica aerogels. Ammonia adsorption at 50°C, after dehydration of the samples at 300°C, resulted in strong ν(NH) vibrations in the 3400- to 2400 cm^{-1} region (Fig. 1). No vibrations from the bulk catalyst interfere in this region. The total amount of adsorbed ammonia decreased in the order Md/NN > M/NN > M/Tri > M/NC > M/NH_3 > E/NH_3d ≅ E/NH_3. For comparison a pure silica aerogel was investigated. The ammonium ions observed in the presence of gaseous ammonia immediately desorbed in pure argon atmosphere. All mixed oxide aerogels showed Lewis-bound ammonia (L in Fig. 1), with the stretching vibrations in the range 3381–3387 cm^{-1} (ν_{as}(N–H)) and 3276–3287 cm^{-1} (ν_s(N–H)) (35–37). The antisymmetric deformation vibration was observed at 1609 cm^{-1}. During TPD the N–H stretching vibrations shifted to lower wavenumbers, indicating the presence of sites with different acidity on the catalyst. Strongly bound ammonia at 300°C was associated with bands at 3342–3357 cm^{-1} (ν_{as}(NH)) and 3250–3274 cm^{-1} (ν_s(NH)), whereas at room temperature the bands were found at 3381–3387 and 3276–3287 cm^{-1}, respectively (Fig. 2). A correlation of the stretching band position with the acidity of the metal center was also found by Nakamoto for amine complexes (38). The vibration at 3180 cm^{-1} was assigned to the overtone of the δ_{as}(NH) of the stronger bound Lewis species, in Fermi resonance with the nearby stretching vibration ν_s(NH) (37, 39), whereas the band at 3210 cm^{-1} was attributed to the overtone vibration of the weakly bound Lewis species (40), which is strongly supported by the fact that at 300°C the latter band almost completely vanished (Fig. 2).

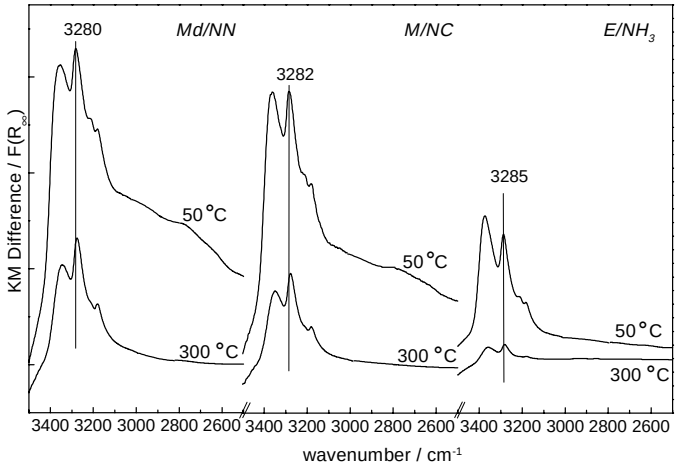

FIG. 2. DRIFTS spectra of ammonia adsorption at 50 and at 300°C on the dehydrated aerogels Md/NN, M/NC, and E/NH_3.

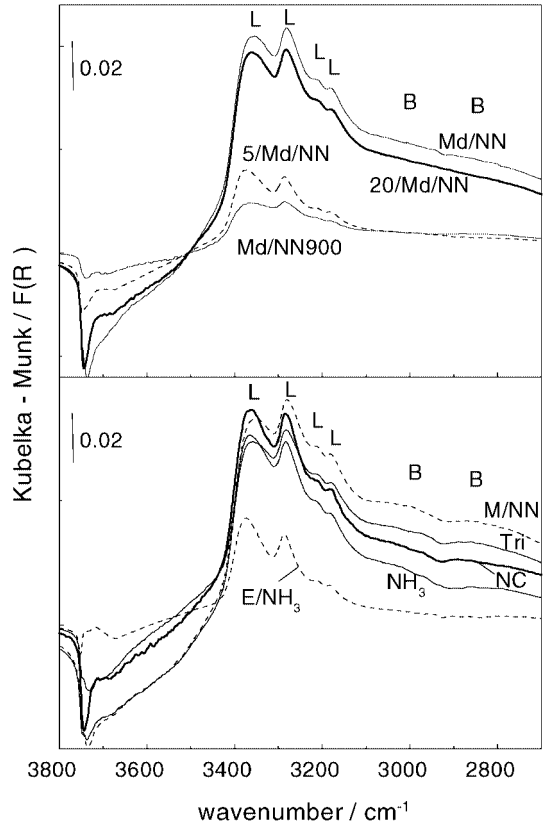

FIG. 1. DRIFTS spectra of ammonia adsorption at 50°C on the dehydrated aerogels. L and B indicate bands mainly associated with Lewis- and Brønsted-bound ammonia, respectively. The aerogel denotations are related to the synthesis conditions and iron content. Top: Aerogels prepared by *N*,*N*-diethylaniline (NN) and a diluted solution of TMOS (Md), with varying iron content corresponding to 5 wt% (5/Md/NN), 10 wt% (Md/NN), and 20 wt% Fe_2O_3 (20/Md/NN), respectively. The denotations without any starting numeral indicate that 10 wt% Fe_2O_3 was used. Md/NN900 corresponds to sample Md/NN calcined at 900°C. Bottom: Aerogels prepared using the N bases: NN = *N*,*N*-diethylaniline, Tri = trihexylamine, NC = ammonium carbonate–water solution, NH_3 = aqueous ammonia solution, and TMOS as silicon precursor. For E/NH_3 TEOS was used.

Brønsted acid properties. Brønsted-bound ammonia is characterized by the broad band at 3200–3000 cm^{-1} (B, in Fig. 1). It is mainly composed of the symmetric and antisymmetric stretching vibrations of adsorbed NH_4^+. A combination band of the symmetric and antisymmetric deformation vibration of NH_4^+ species may arise around 3000 cm^{-1}. The broad vibration around 2800 cm^{-1} is likely associated with the overtone of δ_{as}(NH) (38, 41). The presence of stretching vibrations due to ammonium ions in the 3400- to 3200-cm^{-1} region, where Lewis-bound ammonia also appears, cannot be fully excluded, as narrow bands above 3300 cm^{-1} were assigned to the free N–H groups of adsorbed NH_4^+ on H-ZSM-5, in agreement with *ab initio* calculations (42–44). However, the ν(NH) extinction coefficient of the free N–H is expected to be lower than that of hydrogen-bonded N–H (42, 45). Therefore the intense vibrations observed in our study in the region 3400–3250 cm^{-1} are assigned to Lewis-bound ammonia.

As also reported by Zecchina *et al.* (42), the decrease in intensity of the OH stretching vibrations (negative bands) was correlated with the intensity of the Brønsted bands. The catalysts M/NN, Md/NN, and M/Tri showed the highest decrease in hydroxyls as well as the highest amount of Brønsted-bound ammonia, followed by M/NC and M/NH_3. E/NH_3 and E/NH_3d showed nearly no Brønsted sites and only few hydroxyls were consumed. The acid hydroxyl groups have already been characterized in the previous work (11).

The ratio $A = N_{300}/N_{50}$ of the amount of ammonia adsorbed at 300°C (N_{300}) and 50°C (N_{50}), respectively, derived from the integrated ν(N–H) band areas, was taken as a measure of the mean acidity of the catalysts. The values, listed in Table 2, vary from 9 to 18%. The mean acidity of the catalysts increased in the series $E/NH_3d < E/NH_3 < M/NH_3 < M/NC < M/Tri \cong Md/NN < M/NN$.

The stretching vibrations of ammonia adsorbed at 50°C on the Md/NN aerogels with different iron loading and on Md/NN900 are depicted in the upper part of Fig. 1. The amount of Brønsted-bound ammonia decreases in the order Md/NN > 20/Md/NN > 5/Md/NN ≅ Md/NN900 and correlates well with the amount of hydroxyl groups on the catalysts (11). The stretching vibrations of Lewis-bound ammonia appeared at 3372–3350 and 3286–3280 cm^{-1}. The ratio of ammonia adsorbed at 300 and at 50°C was again determined as a measure for the mean acidity. The values decrease in the series Md/NN > 20/Md/NN > 5/Md/NN > Md/NN900 (Table 2).

NO adsorption on the reduced catalysts. The adsorption studies of NO on the reduced iron oxide–silica aerogels clearly demonstrate the existence of various adsorption sites. Figure 3 shows the spectra of NO adsorbed at steady state under argon at 25°C. Two broad bands can be distinguished at 1830–35 and 1754–58 cm^{-1}, respectively. Yuen *et al.* (46), Segawa *et al.* (47), and Aparicio *et al.* (48) studied the adsorption of NO on silica-supported iron (Fe^{2+}/SiO_2) and Fe(II)-Y zeolite. The authors could assign NO stretching bands to NO adsorbed on differently coordinated iron by comparison with Mössbauer spectroscopy. The vibrations at 1870–30 cm^{-1} were assigned to highly coordinated iron with low or intermediate accessibility for NO to adsorb, whereas the vibrations at 1750 and 1767 cm^{-1} were assigned to a mononitrosyl of Fe^{2+} in a low-coordinated state. For iron on amorphous silica (2) the ν(NO) at 1755 cm^{-1} was assigned to NO adsorbed on Fe^{2+} incorporated in the silica. We therefore assign the band at 1830–35 cm^{-1} to NO adsorbed on Fe^{2+} with high coordination, probably incorporated in small iron oxide clusters, with a broad dispersion of sites due to differences in coordination and/or accessibility. The band around 1755 cm^{-1} is assigned to low-coordinated Fe^{2+}, probably due to iron incorporated in the silica matrix. Table 2 lists the ratio, $R = Fe_{low}{}^{2+}/ Fe_{high}{}^{2+}$, of low- to high-coordinated Fe^{2+}, determined by the integrated area of the corresponding ν(NO) band. The ratio R decreases in the series M/NN > M/Tri > M/NC ≅ M/NH_3 > E/NH_3.

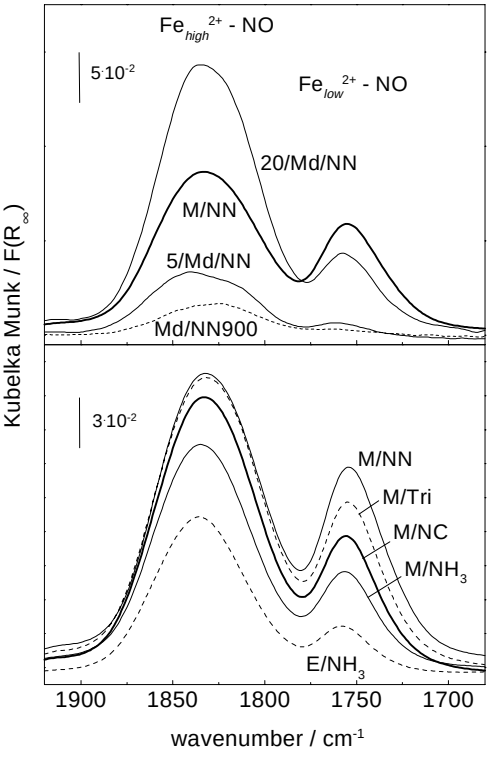

FIG. 3. DRIFT spectra of steady-state NO adsorption under argon at room temperature on the aerogels, reduced at 425°C in hydrogen. Top: spectra of the aerogels with different iron content are shown. Bottom: spectra of the aerogels prepared by different N-bases are depicted.

TABLE 2

Results from Ammonia and NO Adsorption Studies [a]

Catalyst	N_{50} [b]	N_{300} [b]	$A = N_{300}/N_{50}$	R [c] $= Fe_{low}{}^{2+}/Fe_{high}{}^{2+}$
Md/NN	54	9	0.166	—
Md/NN900	11	0.5	0.045	0.113
5/Md/NN	13	1	0.077	0.121
20/Md/NN	47	6	0.128	0.163
M/NN	47	8	0.176	0.457
M/Tri	38	6	0.164	0.35
M/NC	36	5	0.148	0.29
M/NH_3	27	3	0.116	0.272
E/NH_3	10	1	0.09	0.142
E/NH_3d	11	1	0.09	—

[a] Ammonia uptake of calcined aerogels at 50°C (N_{50}) and 300°C (N_{300}), respectively. Ratio $A = N_{300}/N_{50}$, as determined by DRIFTS. Relative amount of NO bound to low- and high-coordinated iron, $R = Fe_{low}{}^{2+}/Fe_{high}{}^{2+}$, on reduced aerogels.

[b] Area of the ν(NH) vibrations of ammonia in the range 3500–2000 cm^{-1}.

[c] Ratio of the area of the ν(NO) band at 1755 and 1830 cm^{-1}.

NO adsorption on the reduced aerogels with different iron content and calcination temperature is shown in Fig. 3 (top). The highest amount of NO adsorbed was observed on 20/Md/NN, followed by M/NN; very little was adsorbed on 5/Md/NN and Md/NN900. The ratio R of the integrated area of the ν(NO) band on low- and high-coordinated Fe^{2+} decreases in the series Md/NN > 20/Md/NN > 5/Md/NN ≅ Md/NN900 (Table 2).

3.3. Selective Catalytic Oxidation (SCO) of Ammonia

Catalytic tests. The results of the catalytic tests in the SCO of ammonia measured in the 210–550°C range are summarized in Table 3. High selectivity to nitrogen up to 98% combined with full conversion of ammonia could be achieved at 500°C for M/NN, Md/NN, M/Tri, and M/NC. M/NH_3, E/NH_3, and E/NH_3d afforded a selectivity of 90 to 93% N_2 at 540°C, with N_2O and NO as by-products. Activity decreased in the order Md/NN > M/NN > M/Tri > M/NC > M/NH_3 > E/NH_3d > E/NH_3, as reflected by both TOF and rate per surface area at 330°C (Table 3, Fig. 4 bottom). Note that the reported TOF values are conservative estimates (lower limit), since for their calculation the total amount of iron was considered. The highest activity showed the aerogels prepared with *N*,*N*-diethylaniline as gelation agents, Md/NN and M/NN, with a TOF of 0.16 and 0.14 $(ks)^{-1}$, respectively. Catalysts M/Tri, M/NC, and M/NH_3 were considerably less active (TOF = 0.08 − 0.06 $(ks)^{-1}$). E/NH_3 and E/NH_3d were the least active catalysts (TOF ≅ 0.05 $(ks)^{-1}$). Reference measurements with the silica component alone showed some activity, reaching 5% conversion at 500°C with selectivity to NO of 57%. Among the catalysts with different iron content the activity decreased in the order Md/NN > 5/Md/NN ≫ 20/Md/NN. Note that the rate per surface area of the 5% Fe_2O_3-containing aerogel (5/Md/NN) is lower than expected from the TOF value because the surface area of this sample was nearly two times higher than that of the other aerogels. The activity collapsed for the 20/Md/NN catalyst, whereas the selectivity was still very high, amounting to 97% at 500°C (X > 98%). The Md/NN900 aerogel, calcined at 900°C, was less active than the corresponding aerogel calcined at 600°C. This can only partly be explained by the decrease in surface area. The rate per surface area was indeed only 15% lower compared to that for Md/NN. The Arrhenius plots are shown in Fig. 4. The activation energies ($E(N_2)$) calculated from the differential measurements were in the range 69–94 kJ mol^{-1}, the catalysts with the higher selectivity and activity showing lower activation energies.

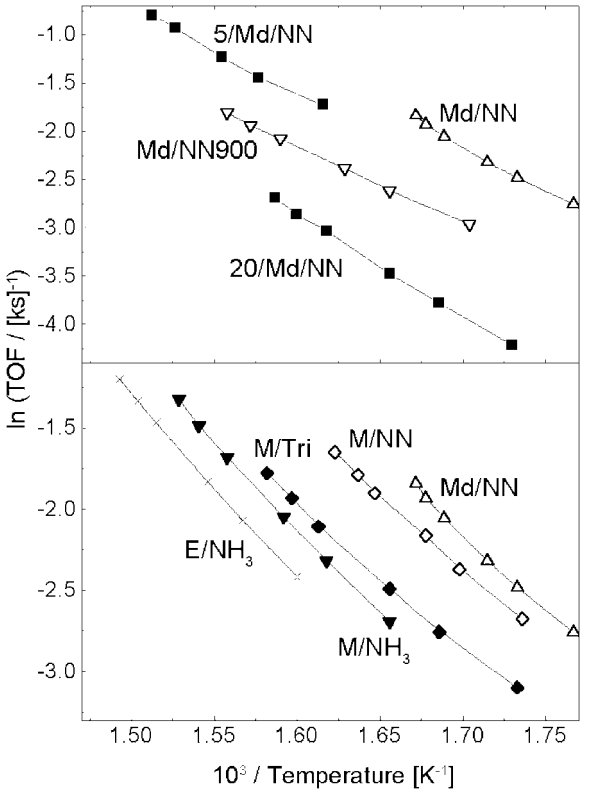

FIG. 4. SCO of ammonia. Arrhenius plot of N_2 production rates for aerogels prepared by different sol–gel synthesis. Top: aerogels with different iron content and calcination temperature. Bottom: aerogels containing 10 wt% nominal Fe_2O_3 prepared by different N bases.

TABLE 3

Catalytic Results of the Iron Oxide–Silica Aerogels in the Selective Catalytic Oxidation of Ammonia to N_2

Catalyst	$E_{act}(N_2)$ (kJ mol^{-1})	TOF[a] × 10^6 (s^{-1}) (330°C)	Rate × 10^{11} (mol N_2 m^{-2} s^{-1}) (330°C)	Selectivity to N_2 (%) (X > 98%, 500°C)
Md/NN	80 ± 4[b]	164[c]	68[b]	96
Md/NN900	69 ± 5	72	58	93
5/Md/NN	86 ± 3	103[c]	11[c]	96[d]
20/Md/NN	90 ± 5	31	19	97
M/NN	79 ± 5	137	55	97
M/Tri	77 ± 5	80	30	97
M/NC	76 ± 3	70	24	97
M/NH_3	90 ± 5	64[c]	22[c]	90[d]
E/NH_3	94 ± 4	48[c]	10[c]	93[d]
E/NH_3d	94 ± 4	51[c]	11[c]	91[d]

[a] TOF = $[N_2]/([Fe] \cdot s)$.

[b] Ninety-five percent confidence limits of Arrhenius-type linear regression.

[c] Extrapolated values.

[d] X > 98% at 540°C.

The selectivity to nitrogen varied with temperature and was highest at 450–540°C. The selectivities to the by-products NO and N_2O, for the catalysts with highest (Md/NN) and lowest activity (E/NH_3), are depicted in Fig. 5 (right). The upper plot is characteristic also for aerogels M/NN, M/Tri, and M/NC. Selectivity to N_2O amounted to 8–10% and was higher than that to NO up to 330°C. At higher temperature NO selectivity increased to about 5%

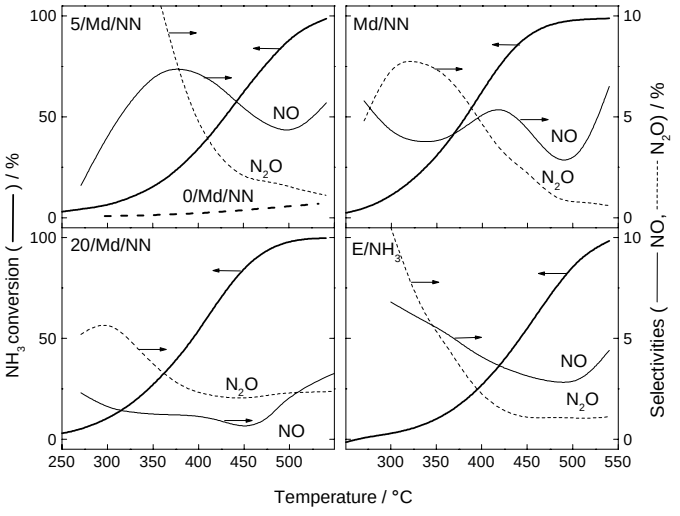

FIG. 5. SCO of ammonia. Conversion of ammonia and selectivities to nitrous and nitric oxide for catalysts 5/Md/NN and 20/Md/NN (left) and Md/NN and E/NH_3 during the integral reactivity studies. For comparison, ammonia conversion with the pure silica aerogel (0/Md/NN) is shown in section 5/Md/NN.

at the expense of N_2O. Between 400 and 480°C both by-products nearly disappeared, and N_2 selectivity reached a maximum. Selectivities to NO and N_2O for E/NH_3 (Fig. 5, right), M/NH_3, and E/NH_3d decreased steadily with increasing temperature. Again with high conversion at 500°C they nearly disappeared. Comparing the aerogels with different iron contents, a decrease in the formation of by-products with higher iron loading was observed.

Catalytic activity was investigated also for Md/NN after *in situ* reduction at 550°C in 5% H_2/Ar. The catalyst showed about half the activity of the calcined one, its selectivity to N_2 increased in the 320–440°C range, and only small amounts of N_2O were produced. Above 450°C NO production increased, reaching 14% at 540°C, which is twice the value found for the calcined catalyst.

In situ DRIFTS measurements during SCO of ammonia. DRIFTS was used to investigate the role of the acidic sites in the SCO of ammonia. For this purpose M/NN and E/NH_3 were pretreated in air, and then ammonia was adsorbed at 250°C. The observed bands corresponded to Lewis- and Brønsted-bound ammonia. Figure 6 depicts the disappearance of ammonia after admission of 1.8% O_2/Ar at 250°C for catalyst M/NN (top) and E/NH_3 (bottom). With both catalysts admission of oxygen led to an immediate decrease of the Lewis-bound ammonia, characterized by the vibrations at 3400–3200 cm^{-1} (ν(NH)) and 1608 cm^{-1} (δ(NH)). Concurrently an increase of the signal in the region 3700–3500 cm^{-1} was observed, probably due to hydroxyls hydrogen bonded to water (34). On M/NN the admission of oxygen led also to an increase of a broad band at 3000–2800 cm^{-1} together with a vibration at 1440 cm^{-1} during the first 10 min. This effect was not so distinct on E/NH_3. Brønsted-bound ammonia was formed or rearranged due to the water produced during SCO. After 30 min some of the Brønsted-bound ammonia started to react. It must be pointed out that only a slight decrease in these bands was observed compared to the vibrations due to the Lewis-bound ammonia.

The position of the vibrations of the consumed Lewis-bound ammonia was nearly constant over the whole reaction time at 3330 cm^{-1} (ν_{as}(NH)), 3370 cm^{-1} (ν_s(NH)), and 3172 cm^{-1} (overtone of the δ(NH)) on M/NN and at 3340, 3373, and 3174 cm^{-1} on E/NH_3. In both cases the frequency of the stretching vibration of the reacted ammonia was lower than that of the adsorbed species, indicating that the more acid Lewis species had reacted (cf. ammonia adsorption studies). Brønsted-bound ammonia was consumed at 2600 cm^{-1} on M/NN and 2730 cm^{-1} on E/NH_3. Also in this case the frequency of the consumed ammonia was lower than that of the Brønsted species before reaction (2785 and 2810 cm^{-1}, respectively). Broad bands associated with the deformation vibrations of these species were observed at 1700 and 1450 cm^{-1}.

TPD and reduction by ammonia after different pretreatments of the aerogels. TPD in helium (SCO–TPD) was performed for all samples after the catalytic test in SCO. The desorption signals of NH_3, N_2, NO, and N_2O are

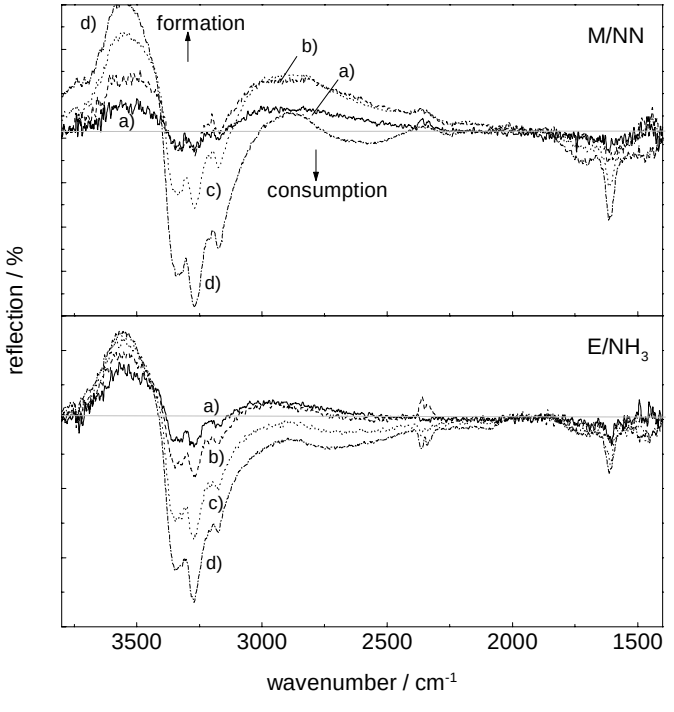

FIG. 6. DRIFTS study of the reaction of preadsorbed ammonia with oxygen at 250°C. Spectra were recorded after (a) 4, (b) 10, (c) 30, and (d) 60 min. Spectra of adsorbed ammonia in argon at 250°C (0 min) was substracted.

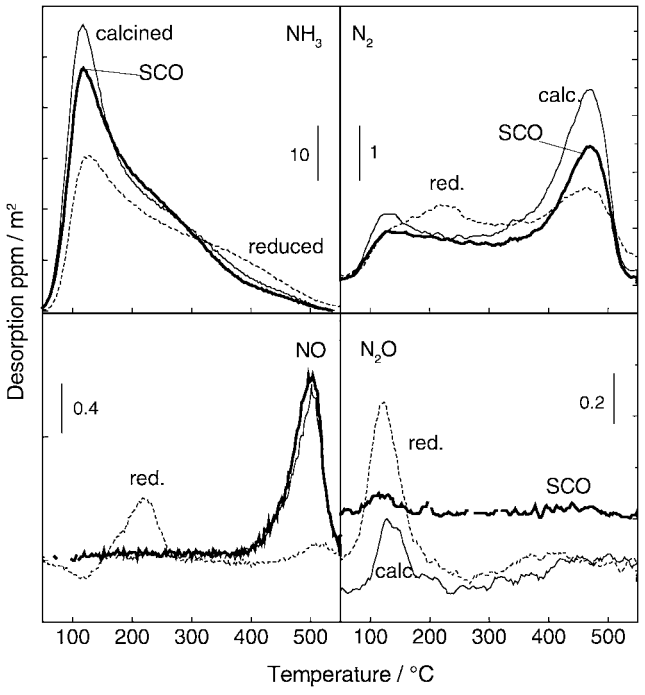

FIG. 7. TPD of ammonia from differently pretreated catalyst Md/NN. After *in situ* calcination (thin line), after use in SCO (thick line), and after *in situ* reduction in 5% H_2/He at 550°C (dashed line).

representatively shown for differently pretreated catalyst Md/NN in Fig. 7. For all aerogels desorption of ammonia showed a maximum at 105–119°C and was observed up to 500°C. The overall amount of desorbed ammonia decreased in the series M/NN ≅ Md/NN > M/Tri > M/NC > M/NH_3 > E/NH_3d ≅ E/NH_3, and corresponded well to the amount of adsorbed ammonia determined by DRIFTS for the calcined samples. N_2 and NO were found to desorb at temperatures above 390°C, whereas N_2O was not observed. The desorption of N_2 and NO was maximal at 460–480°C. Water desorption was prominent in the 170–200°C range for the samples which showed high Brønsted acidity in DRIFTS (Md/NN, M/NN, M/Tri), whereas on the other samples it was shifted to lower temperature. The concurrent desorption of ammonia and water at higher temperature may therefore be attributed to the desorption of stronger Brønsted-bound ammonia followed by condensation of the hydroxyl groups. Ammonia desorption can originate from Brønsted- and Lewis-bound ammonia up to 300°C, as shown by DRIFTS.

Aerogel Md/NN was also investigated after calcination in air at 550°C and after reduction in hydrogen at 550°C (Fig. 7). The desorption profiles for ammonia and N_2 were slightly more intense with the calcined catalyst compared to that used in SCO. All curves had similar shapes to those observed after use in SCO. For the reduced catalyst, however, distinct differences in the desorption behavior were observed: ammonia desorption decreased, N_2O desorption at low-temperature (120°C) became prominent, and some NO and N_2 desorbed at 220°C. At high temperature nearly no oxidation products were observed, but ammonia desorption was slightly increased compared to the calcined sample.

The reduction of the catalysts by ammonia was investigated using *in situ* TPR with NH_3 for M/NH_3, E/NH_3, and Md/NN. Upon heating in 2000 ppm NH_3/He, the nitrogen production started at about 280°C (not shown). The maximum N_2 production occurred at 460–468°C. Only N_2 and water were produced during reduction, whereas during reaction with oxygen and also during TPD, products of deeper oxidation were observed. The amount of nitrogen formed was higher after use in SCO than after calcination, which may be explained by the presence of adsorbed intermediate species from the catalytic reaction.

3.4. Selective Catalytic Reduction of NO with NH_3

The Arrhenius plot of the mixed oxide aerogels in SCR of NO with ammonia is shown in Fig. 8. Additionally the catalytic performance of the aerogels is summarized in Table 4. Note that the activity of the aerogels is compared at a temperature where only SCR occurred (210°C). The activity was highest for aerogel E/NH_3 with a TOF amounting to 0.12 N_2 Fe^{-1} ks^{-1}, followed by M/NH_3 (0.11 N_2 Fe^{-1} ks^{-1}). M/NC, M/Tri, and M/NN showed lower activity with about 0.08 N_2 Fe^{-1} ks^{-1}. In general the activity was higher than that in the SCO of ammonia. The selectivity toward nitrogen was high over the whole temperature range studied, and amounted to 98–99% in the 380–460°C range ($S_{N_2} + S_{N_2O} = 1$), that is, when the catalysts reached >98% conversion of ammonia. The consumption of NO decreased at temperatures higher than 250°C, due to the onset of ammonia oxidation. The ratio of the conversion of NO and NH_3 (X_{NO}/X_{NH_3}) decreased with higher temperature. Among the aerogels studied it decreased in the series

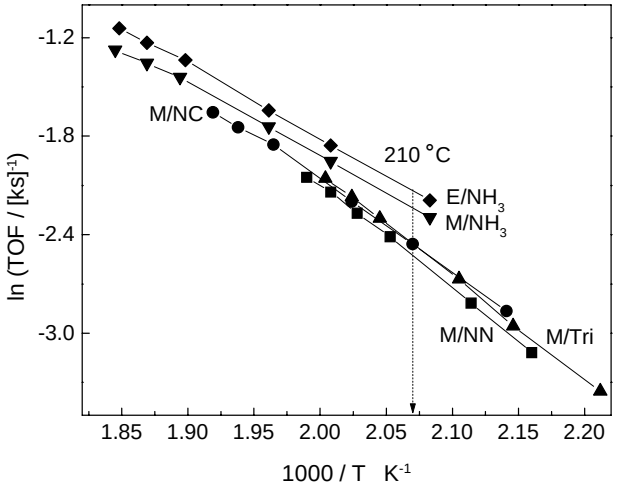

FIG. 8. Temperature dependence of SCR of NO by ammonia on various aerogels. Arrhenius plot of the N_2 production rates.

TABLE 4

Catalytic Results of Iron Oxide–Silica Aerogels in the Selective Catalytic Reduction of NO by Ammonia

Catalyst	E_{act} (N_2) (kJ mol^{-1})	TOF[a] $\times 10^6$ (N_2Fe^{-1} s^{-1}) (210°C)	Rate[a] $\times 10^{11}$ (mol N_2 m^{-2} s^{-1}) (210°C)	Selectivity to N_2[b] (%) ($X > 98\%$, 380–460°C)
M/NN	53 ± 2[c]	80	32	99
M/Tri	46 ± 4	85	32	99
M/NC	47 ± 3	85	35	98
M/NH_3	38 ± 1	106	28	99
E/NH_3	38 ± 2	119	23	98

[a] $X_{NO}/X_{NH_3} = 1$.
[b] $S_{N_2O} = 1 - S_{N_2}$.
[c] Ninety-five percent confidence limits of Arrhenius-type linear regression.

$E/NH_3 > M/NH_3$, M/NC, M/Tri > M/NN, and was therefore inversely correlated to their activity in the SCO of ammonia (Fig. 9). Note, that the influence of the ammonia oxidation sharply increased above 450°C, as seen by the decrease in slope of the NO conversion.

4. DISCUSSION

The following discussion focuses on the correlation between structural and acidic properties of the catalysts and their performance in SCO and SCR.

The catalysts showed distinctly different acidic properties. The DRIFTS results revealed that both the amount of adsorbed ammonia and the strength of adsorption varied considerably among the catalysts. The amount of adsorbed ammonia increased in the series $E/NH_3 \cong E/NH_3d < M/NH_3 < M/NC < M/Tri < M/NN < Md/NN$. At 300°C mainly

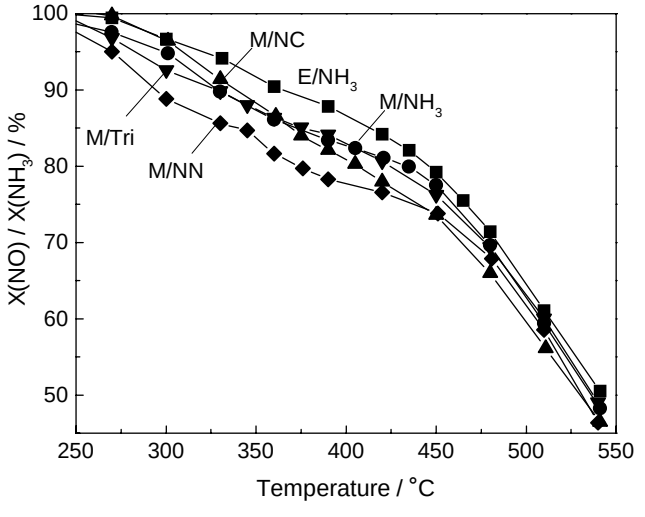

FIG. 9. Selective catalytic reduction of NO by ammonia. Ratio of the NO conversion to the ammonia conversion in the temperature 270–540°C range.

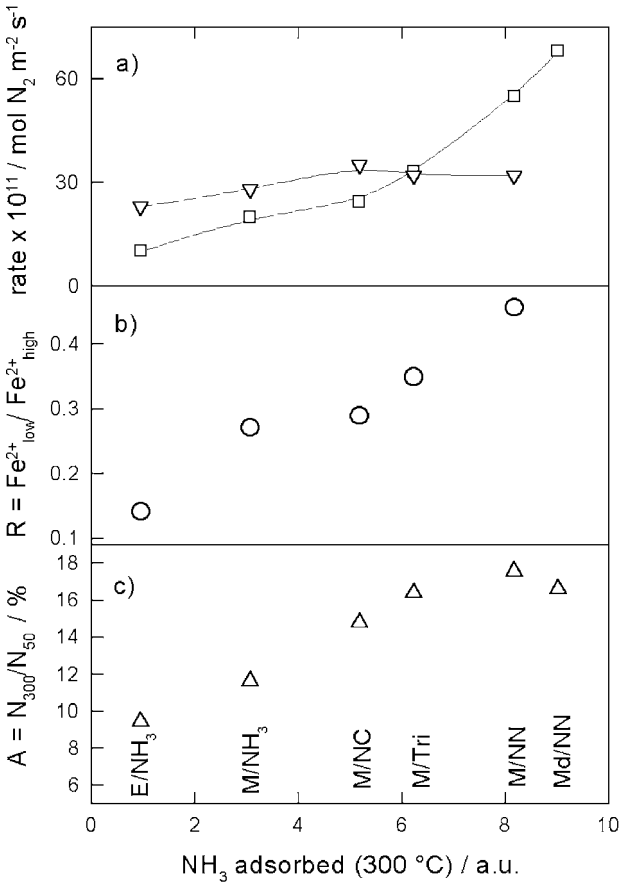

FIG. 10. (a) Correlation between reaction rates of SCO at 330°C (□), SCR at 210°C (▽), and ammonia adsorbed at 300°C. (b) Abundance of low-coordinated iron ($R = Fe_{low}^{2+}/Fe_{high}^{2+}$). (c) Relative amount of strongly bound ammonia ($A = N_{300}/N_{50}$) to total ammonia uptake at 300°C for all aerogels containing 10 wt% Fe_2O_3.

Lewis-bound ammonia was still bound to the surface. The activity in SCO is depicted as a function of the total amount of ammonia adsorbed at 300°C in Fig. 10. Clearly the activity of the catalyst positively correlates with the amount of adsorbed ammonia. Figure 10 also demonstrates that the relative abundance of strongly bound ammonia $A = N_{300}/N_{50}$ increases with increasing adsorption capacity. Both acidity and adsorption capacity for ammonia may play important roles in the oxidation of ammonia. Indeed, for the oxidation of ammonia on Md/NN and E/NH_3 followed by DRIFTS (Fig. 6), the reaction was found to proceed mainly by consumption of the stronger Lewis-bound ammonia. Lewis-bound ammonia was also suggested to be the active species in ammonia oxidation in previous studies for supported and pure iron oxide catalysts (29, 31) and for Cu-exchanged zeolites (49). The best results reported to our knowledge were achieved with ion-exchanged zeolites containing highly dispersed iron (27) or copper ions (49), reaching TOF values of 14 $(ks)^{-1}$ at 350°C and 4.8 $(ks)^{-1}$ at 180°C, respectively.

We propose that the stronger Lewis-bound ammonia is associated with isolated Fe ions, embedded in the silica matrix in tetrahedral coordination, whose relative abundance, *R*, grows parallel to the relative amount of strongly bound ammonia, as indicated in Figs. 10b and 10c. These sites are in low coordination in contrast to the iron ions in agglomerates (46, 48, 50) and could be characterized by NO adsorption on the reduced aerogels. The presence of tetrahedrally coordinated Fe^{3+} has been evidenced by UV–vis and EPR spectroscopy on the calcined samples (11). The dispersion of the iron ions decreased in the series M/NN > M/Tri > M/NC ≅ M/NH_3 > E/NH_3. Also compared to the aerogels 5/Md/NN, 20/Md/NN, and Md/NN900, the relative amount of low-coordinated iron was greater on M/NN and Md/NN. Tetrahedral coordination of Fe^{3+} in the silica leads to strong Lewis acid centers, as well as Brønsted acid Fe^{3+}–OH–Si groups, as known from studies on zeolites (51, 52).

NO adsorption studies showed that iron oxide nanoparticles were relatively more abundant on E/NH_3 than on M/NN (Table 2, Fig. 3), in agreement with UV–vis and EPR spectroscopy (11). Rethwisch and Dumesic (2) assigned the vibration at 1830 cm^{-1} to NO bound to iron oxide particles on amorphous silica. The particle size increased with higher calcination temperature (Md/NN900) and with increasing iron content (20/Md/NN), as shown in our previous study by EPR and XRD (11). On these samples also crystalline iron oxide particles were detected. The abundance of acidic sites and their strength were lower on these catalysts; on hematite only weak acid sites were observed, and nearly no ammonia adsorption was found at 300°C (not shown). Correspondingly, catalysts with a high abundance of iron oxide nanoparticles showed low activity in SCO (Fig. 4). On the other hand, no loss in selectivity toward N_2 was observed up to 550°C for the catalysts with high content of iron oxide particles. For Md/NN900 the same selectivities as those on Md/NN were observed, whereas on 20/Md/NN, N_2 selectivity was even higher in the low-temperature range (Fig. 5). These results are supported by earlier SCO studies on pure hematite, which revealed low activity compared to that on other transition metal oxides (31, 32).

Iron oxide supported on silica was investigated by Uddin *et al.* (16), but low selectivity toward nitrogen was observed. On MFI-type ferrisilicalite (16) and Fe/Al_2O_3 (3), selectivity to N_2 > 90% in the 400–500°C range was obtained. Long and Yang (27) investigated SCO on Fe-exchanged zeolites and reported high activity with selectivity toward nitrogen reaching 100% at 450°C. At this temperature a TOF value of 22 $(ks)^{-1}$ was observed for Fe-ZSM-5 with 0.86 wt% Fe. Note that H-ZSM-5 is also active in SCO (53). Increasing the Si/Al ratio in Fe-ZSM-5 from 10 to 100, 20% loss in activity and up to 50% lower selectivity to N_2 were observed.

The activation energy for N_2 formation in SCO for the aerogels is in the range 80–90 kJ/mol. Similar values were obtained for V_2O_5/SiO_2 (54) and Fe-ZSM-5 (27), whereas a lower activation energy was found for Pt catalysts (55). The activation energy for pure hematite amounted to 95–100 kJ/mol (31, 32) and was close to that of our less active samples. The activation energy was lower for the more active catalysts M/NC, M/Tri, M/NN, and Md/NN than for M/NH_3, E/NH_3, and E/NH_3d (Table 3). The catalysts with low activation energy possess larger acidity than the catalysts with high activation energy (Fig. 10). The acidity and hence the adsorption strength of the ammonia may play important roles in the dehydrogenation step of ammonia. Amide species as intermediate toward N_2 production were also postulated by Amores *et al.* (28) for supported transition metal oxides and by Williamson *et al.* for Cu-Y (49), whereas dimerization of NH_2O species was suggested to occur over molybdena supported on silica (54). On pure oxides Matyshak and Krylov (32) and Il'chenko and Golodets (31) proposed the reaction of an amide with a nitro/HNO species to form nitrogen.

For SCO the selectivity toward nitrogen increases at higher temperature (Fig. 5), as also reported by Long and Yang (27) for Fe-ZSM-5 and by Amblard *et al.* (3) for Ni/Al_2O_3, Mn/Al_2O_3, and Fe/Al_2O_3, on which N_2 production was maximal at 350–550°C depending on the transition metal investigated and decreased at higher temperature due to NO production. We observed an increase in NO above 500°C, which was more pronounced on Md/NN prereduced at 550°C than on the calcined sample. Reaction on the pure SiO_2 aerogel, producing mainly NO, has to be taken into account at this temperature, but its activity was too low to fully explain the NO onset on the mixed oxide aerogels. The presence of iron oxide agglomerates did not lead to formation of large amounts of by-products, as demonstrated by the high selectivity to nitrogen observed for Md/NN/900 and 20/Md/NN over the whole temperature range studied. Hence the observed increase in selectivity toward NO above 500°C is likely not associated with iron oxide agglomerates. A possible pathway for N_2O formation at low-temperature is the combination of an adsorbed dehydrogenated ammonia species with NO (54) or an adsorbed nitro/nitrate species. Alternatively the combination of two adsorbed HNO species was postulated (31). Nearly no N_2O was observed during SCR, rendering the internal SCR mechanism less probable.

We observed NO production also during the TPD of ammonia in argon above 400°C. The catalyst is therefore easily reduced above this temperature. On the other hand, TPR in ammonia showed only formation of N_2. This indicates that an increased surface coverage of ammonia suppresses NO formation at high temperature. Differential catalytic measurements in SCO in the 350–400°C range revealed that the activation energy for NO formation was about 120–150 kJ/mol, much higher than that for N_2 and N_2O formation with activation energies between 70 and

90 kJ/mol. The values for the activation energies explain the onset in NO production at higher temperature. Therefore oxidation of ammonia to NO and reaction of NO with adsorbed ammonia (internal SCR), as suggested by Long and Yang (27) for Fe-ZSM-5, are likely not the dominant route for N_2 production in SCO on our catalysts. This is further supported by the different activity in SCO and SCR for the catalyst series investigated.

The activity of the catalysts in SCR does not correlate with their activity in SCO (Fig. 10). The reaction rate per surface area for SCR only increases slightly with increasing ammonia adsorption capacity. The different influence of the acidity on the activity indicates that the active sites for SCR differ from those for SCO. Based on the observation that the samples containing a substantial amount of iron oxide clusters showed a consistently higher SCR activity, we may infer that these species are important for SCR. Joyner and Stockenhuber (56) reported that on Fe-ZSM-5 iron oxide nanoclusters were more active for SCR with hydrocarbons than the isolated Fe cations. The activation energies for SCR lie between 38 and 53 kJ/mol (Table 3) and are the same for ammonia and NO conversion and production of nitrogen. Again the more active catalysts have slightly lower activation energies. All activation energies are lower than the values reported for H-ZSM-5 (43, 57) and H-mordenite (58), with activation energies of 60–65 kJ/mol.

In contrast to vanadia catalysts, where no adsorption of NO was observed on the oxidized catalyst, both NO_x and NH_3 may adsorb on iron-containing catalysts (2, 18, 47, 48, 50, 56) as well as on molecular sieve-type catalysts. Formation of NO_2 (or an adsorbed NO_2-like species) followed by reduction by ammonia was proposed to be the main route in the SCR of NO over H-mordenite and H-ZSM-5 (57, 59, 60). Also for Fe-exchanged-pillared clays and Fe-ZSM-5-adsorbed NO_x species were found to be reactive to NH_3 (14, 18). Furthermore the presence of adsorbed ammonia pairs was proposed to increase the catalytic activity in SCR (18, 59).

The influence of SCO on SCR of NO by ammonia was not constant over the temperature range analyzed, mainly as a consequence of the different activation energies of these processes. Ammonia oxidation during SCR started at about 250°C, in agreement with the SCO investigations. The NO conversion steadily decreased relative to the NH_3 conversion above this temperature. At 450°C a distinct decrease in the slope of $X(NO)/X(NH_3)$ versus temperature was observed (Fig. 9). At this temperature NO evolution increased noticeably during ammonia TPD. Hence, the aerogel can be quickly reduced above 450°C, which is reflected in the activity for SCO. However, TPD of ammonia after different pretreatments indicates that the catalyst after use in SCO predominantly maintains the oxidation state of the calcined aerogel, which was determined to be +3 by TPR (11).

5. CONCLUSIONS

Iron oxide–silica aerogels with different iron dispersion ranging from tetrahedrally coordinated Fe^{3+} to iron oxide clusters were synthesized by varying the sol–gel route, the calcination temperature, and the iron content. The aerogels showed high selectivity to nitrogen in the SCO of ammonia, reaching 97% at 500°C. Catalytic oxidation of ammonia in the presence and absence of oxygen started at about 270°C. The SCO activity was found to be positively correlated to the acidity of the aerogels probed by ammonia adsorption. The relative abundance of strong acid sites correlated to the fraction of low-coordinated iron, probably incorporated into the silica matrix. Therefore we propose that the acid sites associated with the low-coordinated iron are the active sites for SCO. Lewis-bound ammonia is likely to be the reactive species for this reaction.

The activity for the SCR of NO by ammonia did not correlate to the Lewis acidity of the iron oxide–silica aerogels, indicating that these sites do not play a crucial role in SCR. In general the activity for SCR was higher than that found for SCO of ammonia. SCO lowered the selectivity to nitrogen achievable by SCR at temperatures higher than ca. 250°C.

REFERENCES

1. Ratnasamy, P., and Kumar, R., *Catal. Today* **9**(4), 329 (1991).
2. Rethwisch, D. G., and Dumesic, J. A., *J. Phys. Chem.* **90**,1625 (1986).
3. Amblard, M., Burch, R., and Southward, B. W. L., *Appl. Catal. B–Environ.* **22**, L159 (1999).
4. Janssen, F. J. J. G., and van den Kerkhof, F. M. G., *KEMA Scientific Tech. Rep.* **3**(6), 71 (1985).
5. Cheng, L. S., Yang, R. T., and Chen, N., *J. Catal.* **164**, 70 (1996).
6. Wang, C. T., and Willey, R. J., *J. Non–Cryst. Solids* **225**, 173 (1998).
7. Willey, R. J., Lai, H., and Peri, J. B., *J. Catal.* **130**, 319 (1991).
8. Willey, R. J., Oliver , S. A., Olivieri, G., and Busca, G., *J. Mater. Res.* **8**(6), 1418 (1993).
9. Hutter, R., Mallat, T., and Baiker, A., *J. Catal.* **153**, 177 (1995).
10. Hutter, R., Mallat, T., Dutoit, D., and Baiker, A., *Top. Catal.* **3**, 421 (1996).
11. Fabrizioli, P., Burgener, M., Bürgi, T., van Doorslaer, S., and Baiker, A., *J. Mater. Chem.*, in press.
12. Bosch, H., and Janssen, F., *Catal. Today* **2/4**, 369 (1987).
13. Long, R. Q., and Yang, R. T., *J. Catal.* **194**, 80 (2000).
14. Long, R. Q., and Yang, R. T., *J. Catal.* **198**, 20 (2001).
15. Amiridis, M. D., Puglisi, F., Dumesic, J. A., Millman, W. S., and Topsoe, N.-Y., *J. Catal.* **142**, 572 (1993).
16. Uddin, M., Komatsu, T., and Yashima, T., *J. Chem. Soc., Faraday Trans.* **91**(18), 3275 (1995).
17. Seiyama, T., Arakawa, T., Matsuda, T., Takita, Y., and Yamazoe, N., *J. Catal.* **48**, 1 (1977).
18. Long, R. Q., and Yang, R. T., *J. Catal.* **190**, 22 (2000).
19. Long, R. Q., and Yang, R. T., *Catal. Lett.* **59**, 39 (1999).
20. Chen, J. P., Hausladen, M. C., and Yang, R. T., *J. Catal.* **151**, 135 (1995).
21. Kato, A., Matsuda, S., Kamo, T., Nakajima, F., Kuroda, H., and Narita, T., *J. Phys. Chem.* **85**, 4099 (1981).
22. Chang, T.-H., and Leu, F.-C., *Appl. Catal. A Gen.* **180**, 123 (1999).
23. Naruse, Y., Ogasawara, T., Hata, T., and Kishitaka, H., *Ind. Eng. Chem. Prod. Res. Div.* **19**, 57 (1980).

24. Biermann, J. J. P., *in* "KEMA Scientific & Technical Reports" (A. J. van Loon, Ed.), Vol. 8(5), p. 273. KEMA, Den Haag, 1990.
25. Heck, R. M., Chen, J. M., and Speronello, B. K., *Environ. Prog.* **13**, 221 (1994).
26. Long, R. Q., and Yang, R. T., *Chem. Commun.* 1651 (2000).
27. Long, R. Q., and Yang, R. T., *J. Catal.* **201**, 145 (2001).
28. Amores, J. M. G., Escribano, V. S., Ramis, G., and Busca, G., *Appl. Catal. B–Environ.* **13**, 45 (1997).
29. Ramis, G., Yi, L., Busca, G., Turco, M., Kotour, E., and Willey, R. J., *J. Catal.* **157**, 523 (1995).
30. Larrubia, M. A., Ramis, C., and Busca, G., *Appl. Catal. B–Environ.* **30**, 101 (2001).
31. Il'chenko, N. I., and Golodets, G. I., *J. Catal.* **39**, 57 (1975).
32. Matyshak, V. A., and Krylov, O. V., *Catal. Today* **25**, 1 (1995).
33. Sil'chenkova, O. N., Matyshak, V. A., and Korchak, V. N., *Kinet. Katal.* **40**, 526 (1999).
34. Vansant, E. F., Van Der Voort, P., and Vrancken, K. C., *Stud. Surf. Sci. Catal.* **93**, 59 (1995).
35. Davydov, A. A., "Infrared Spectroscopy of Adsorbed species on the Surface of Transition Metal Oxides." Wiley, Chichester, 1990.
36. Little, L. H., "Infrared Spectra of Adsorbed Species," p. 180. Academic Press, New York, 1966.
37. Topsoe, N.-Y., *J. Catal.* **128**, 499 (1991).
38. Nakamoto, K., "Infrared and Raman Spectra of Inorganic and Coordination Compounds," Wiley, New York, 1995.
39. Busca, G., Centi, G., Marchetti, L., and Trifiro, F., *Langmuir* **2**, 568 (1986).
40. Pittman, R. M., and Bell, A. T., *Catal. Lett.* **24**, 1 (1994).
41. Vedder, W., and Hornig, D. F., *J. Chem. Phys.* **35** (5), 1560 (1961).
42. Zecchina, A., Marchese, L., Bordiga, S., Pazè, C., and Gianotti, E., *J. Phys. Chem. B* **101**, 10,128 (1997).
43. Eng, J., and Bartholomew, H., *J. Catal.* **171**, 27 (1997).
44. Teunissen, E. H., van Santen, R. A., Jansen, A. P. J., and van Duijneveldt, F. B., *J. Phys. Chem.* **97**, 203 (1993).
45. Pimentel, G. C., and McClellan, A. L., *in* "The Hydrogen Bond" (L. Pauling, Ed.), p. 221. Freeman, San Francisco, 1960.
46. Yuen, S., Chen, Y., Kubsh, J. E., Dumesic, J. A., Topsoe, N., and Topsoe, H., *J. Phys. Chem.* **86**, 3022 (1982).
47. Segawa, K.-I., Chen, Y., Kubsh, J. E., Delgass, W. N., Dumesic, J. A., Hall, W. K., *J. Catal.* **76**, 112 (1982).
48. Aparicio, L. A., Hall, W. K., Fang, S.-M., Ulla, M. A., Millman, W. S., Dumesic, J. A., *J. Catal.* **108**, 233 (1987).
49. Williamson, W. B., Flentge, D. R., and Lunsford, J. H., *J. Catal.* **37**, 258 (1975).
50. Lobree, L. J., Hwang, I., Reimer, J. A., and Bell, A. T., *J. Catal.* **186**, 242 (1999).
51. Datka, J., and Abramowicz, T., *J. Chem. Soc., Faraday Trans.* **90**(6), 2417 (1994).
52. Bordiga, S., Buzzoni, R., Geobaldo, F., Lamberti, C., Giamello, E., Zecchina, A., Leofanti, G., Petrini, G., Tozzola, G., and Vlaic, G., *J. Catal.* **158**, 486 (1996).
53. Long, R. Q., and Yang, R. T., *Chem. Commun.* 1651 (2000).
54. DeBoer, M., Huisman, H. M., Mos, R. J. M., Leliveld, R. G., vanDillen, A. J., and Geus, J. W., *Catal. Today* **17**, 189 (1993).
55. Willey, R. J., and Djuhadi, V. S., *in* "Catalysis 1987" (J. W. Ward, Ed.), p. 435. Elsevier, Amsterdam, 1988.
56. Joyner, R., and Stockenhuber, M., *J. Phys. Chem. B* **103**, 5963 (1999).
57. Stevenson, S. A., Vartuli, J. C., and Brooks, C. F., *J. Catal.* **190**, 228 (2000).
58. Andersson, L. A. H., Brandin, J. G. M., and Odenbrand, C. U. I., *Catal. Today* **4**, 173 (1989).
59. Eng, J., and Bartholomew, H., *J. Catal.* **171**, 14 (1997).
60. Kiovsky, J. R., Koriada, P. B., Lim, C. T., *Ind. Eng. Chem. Prod. Res. Div.* **19**, 218 (1980).